Tribology International 161 (2021) 107095

Contents lists available at ScienceDirect

Tribology International

journal homepage: www.elsevier.com/locate/triboint

Multi-objective optimization of planetary roller screw mechanism based on improved mathematical modelling

Qin Yao [a], Mengchuang Zhang [b,c,*], Yongshou Liu [a], Shangjun Ma [d]

[a] School of Mechanics, Civil Engineering and Architecture, Northwestern Polytechnical University, Xi'an 710129, PR China
[b] School of Civil Aviation, Northwestern Polytechnical University, Xi'an 710072, PR China
[c] Yangtze River Delta Research Institute of NPU, Taicang City 215400, PR China
[d] Shaanxi Engineering Laboratory for Transmissions and Controls, Northwestern Polytechnical University, Xi'an 710072, PR China

ARTICLE INFO

Keywords:
Planetary roller screw mechanism
Load distribution
Improved iteration algorithm
Multi-objective optimization

ABSTRACT

The optimization of obtaining the most uniform load distribution is important for the load carrying capacity design of the planetary roller screw mechanism (PRSM). However, the stiffness matrix of PRSM in traditional method based on the relationship between load and deformation of the thread may be destroyed when threads are no longer in contact due to machining errors, which would bring convergence problem in optimization process. In this paper, the mathematical model is firstly established to overcome the above drawbacks by proposing an improved iterative algorithm. Then, the multi-objective optimization is conducted to search the best designed pitches for the most uniform load distribution on both the screw-roller and nut-roller interfaces, and results are verified by the finite element method.

1. Introduction

Planetary roller screw mechanism (PRSM) is a kind of precision mechanical transmission device composed of screw, nut, rollers, ring gears and retainers, which mainly serves for electro-mechanical actuator to convert rotary motion into linear motion. The number and the total surface area of the contacts between the screw, the rollers and the nut are substantially increased compared to the ball screw design, resulting in larger dynamic and static load carrying capacities of PRSM [1]. The PRSM has been widely used in as all-electric aircraft, space vehicle, robot, machine tools and many other fields [2,3] due to the advantages of long service life, robustness, high stiffness and reliability, especially the high load carrying capacity.

Since the different structural stiffness of screw, roller and nut, the deformation of them is also different after being loaded, and the phenomenon of non-uniform load distribution among the threads of PRSM is inevitable. Uniform load distribution can improve the stability, accuracy and transmission efficiency of PRSM. Conversely, the non-uniform load distribution may cause overload of some threads, which further leads to plastic deformation [4] or premature contact fatigue damage under the cyclic contact stresses of the overloaded thread [5]. Besides, overload will increase the asperity-contact area and friction coefficient, and worsen lubrication, thereby accelerating wear and shortening service life [6]. Furthermore, experimental results have shown that wear, cracks and spalling are more likely to occur under higher load [7,8], and the wear depths are in accordance with the load distribution among threads [9]. Therefore, the load distribution of PRSM is the key to determine its load carrying capacity and service life, which has been widely studied by many researchers.

By regarding the thread profile of roller as effective ball [4–6,10], the load distribution model of PRSM can be established by referring that of the ball screw [11]. Another common method to solve the load distribution of PRSM is the stiffness model, which is inspired by the application of spring network model in solving the load distribution of threaded connection [12]. Jones et al. proposed the direct stiffness method to construct a stiffness model of PRSM, which can be also used to calculate the load distribution including alternative loading conditions and installation configurations [13]. Zhang et al. improved the stiffness model with considering the installation modes, material and structural parameters [14]. The stiffness model can reflect the load distribution characteristics of PRSM more comprehensively, because it not only considers the Hertz contact deformation and axial deformation presented in the effective ball model, but also the thread deformation of the screw, roller and nut. The representative theoretical methods mentioned above are based on the equilibrium conditions of forces and the deformation compatibility relationship. Besides, the modeling of components with specific elements [15–17] and the finite element method (FEM)

* Corresponding author at: School of Civil Aviation, Northwestern Polytechnical University, Xi'an 710072, PR China.
E-mail address: mczhang@nwpu.edu.cn (M. Zhang).

https://doi.org/10.1016/j.triboint.2021.107095
Received 7 February 2021; Received in revised form 26 April 2021; Accepted 12 May 2021
Available online 15 May 2021

Nomenclature

F_{SRi}, F_{NRi}	axial load on the i^{th} thread couples of the screw-roller and nut-roller interfaces
$\Sigma\delta_{Si}$, $\Sigma\delta_{RSi}$	sum of axial deformation of the screw and roller in the i^{th} closed-loop on the screw-roller interfaces
$\Sigma\delta_{Ni}$, $\Sigma\delta_{RNi}$	sum of axial deformation of the nut and roller in the i^{th} closed-loop on the nut-roller interfaces
e_{SRi}, e_{NRi}	sum of pitch error in the i^{th} closed-loop on the screw-roller and nut-roller interfaces
f	load distribution vector
e	pitch errors vector
K	stiffness matrix
ε	pitch deviation vector
K_{SRi}, K_{NRi}	load sharing coefficient of the screw-roller and nut-roller interfaces
K_{SR}, K_{NR}	maximum load sharing coefficient of the screw-roller and nut-roller interfaces
t_{max}, j_{max}	the maximum number of iterations for the external and internal loop
z_{SR}, z_{NR}	number of unloaded thread on the screw-roller and nut-roller interfaces
k_{SRHi}, k_{NRHi}	contact stiffness of the i^{th} thread couples of the screw-roller and nut-roller interfaces
Acc	convergence accuracy
ΔK_{SRi}, ΔK_{NRi}	load sharing coefficient variations of the i^{th} thread couples on the screw-roller and nut-roller interfaces compared with the previous one without pitch errors
P	design variables
$\mathbf{C_x}$	design constants
$f_{SR}(\mathbf{P}, \mathbf{C_x})$	objective function of the screw-roller interfaces
$f_{NR}(\mathbf{P}, \mathbf{C_x})$	objective function of the nut-roller interfaces
f^{max}, f^{min}	maximum and minimum value of objective function
$\mathbf{P}^l$, $\mathbf{P}^u$	lower and upper bound of the design space
S	the population size
M_t, R_t, Q_t	initial population, temporary population and offspring population
$D(i)$	the j^{th} *offspring of the tth generation for the ith design variable*
$P_i^{(j,t+1)}$	the j^{th} offspring of the t^{th} generation for the i^{th} design variable
α_ς	small variation
r_ς	uniformly sampled random number
η_m	coefficient of mutation distribution

[18,19] can also be used to calculate the load distribution of PRSM.

These studies are conducted for the ideal PRSM, however, the inevitable errors will greatly affect the load distribution. Ma [20], Zhang [9] and Lisowski [21] established the load distribution model considering the errors in the relationship of deformation compatibility based on their previous study. Du et al. proposed a mathematic model incorporating the radial load and machining error to calculate the load distribution in two working states [5]. The pitch of screw, roller and nut are not regarded as the independent parameters in these studies. The conclusion obtained by 200 FEM results with random variables shows that the load distribution is mostly affected by the pitch, but the pitch of screw, roller and nut has different sensitivity and contribution to the load distribution [4].

Furthermore, the load distribution optimization of PRSM to get better load carrying capacity for various applications also deserves more attention. Although the uniformity of load distribution can be improved by modifying or redesigning the thread [5,14], the multi-objective optimization of PRSM can more effectively obtain the optimal load

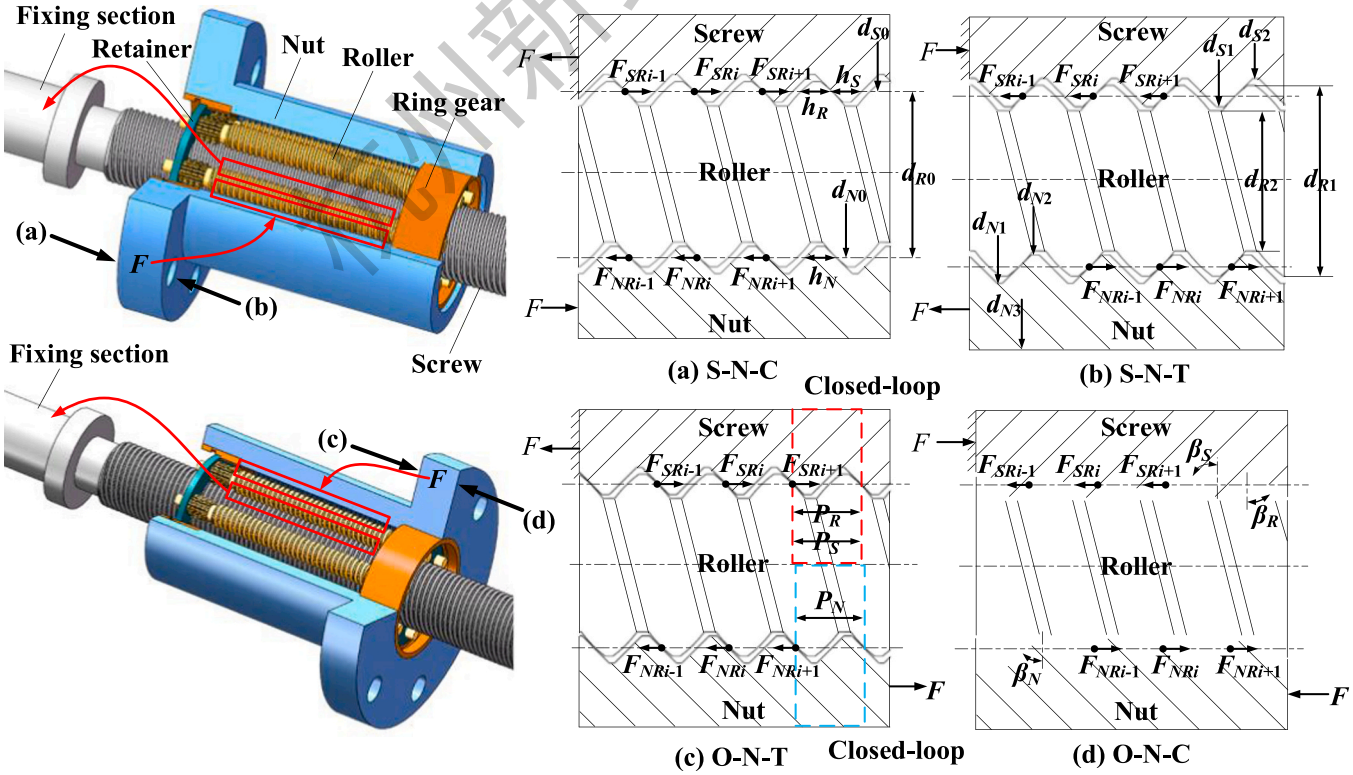

Fig. 1. Schematic diagram of the PRSM in different installation modes.

distribution uniformity on both screw-roller and nut-roller interfaces, which is rarely reported so far. Generally, it is impossible to improve one objective without sacrificing another because they are often in conflict with each other in the multi-objective optimization problem (MOP). The non-dominated sorting genetic algorithm (NSGA-II) [22] is a kind of multi-objective genetic algorithm for solving MOP, which can construct a Pareto front by selecting feasible non-dominated designs and treating each objective separately.

In this paper, the stiffness model, which can better reflect the thread characteristics of PRSM, is adopted to comprehensively reveal the influence of errors on the load distribution. The pitch error is defined as the difference between the pitch of any adjacent threads on the same part and the nominal pitch, which is mainly caused by machining error such as grinding wheel feed speed. Due to the machining error or special differentiating design, the difference of the nominal pitch between roller and screw (nut) is defined as the pitch deviation. By improving the previous load distribution model [9], not only the pitch errors and installation modes, but also the pitch deviations are considered. However, the thread probably not loaded due to these errors. Based on the relationship between load and deformation, the previous methods can not solve the problem of stiffness matrix failure and calculation un-convergence caused by no-load, or the load distribution may no longer satisfies the force equilibrium condition due to the existence of negative values. An improved iterative algorithm for these problems is proposed, and the effect of pitch errors and pitch deviations on load distribution is further studied.

The structure of this paper are assigned as follows. Firstly, the improved mathematical model of load distribution is established in Section 2. Then, in Section 3, the pitches of screw, roller and nut are selected as design variables, and the multi-objective optimization of the load distribution on the screw-roller and nut-roller interfaces is conducted based on NSGA-II. In Section 4, the correctness of the mathematical model and the optimization results are verified by FEM. Finally, the conclusions of this paper are summarized in Section 5.

2. Mathematical modelling

2.1. Load distribution considering pitch deviation and pitch errors

There are two installation configurations of PRSM in the engineering application: the screw and nut are supported at the same or the opposite ends. Each installation configuration has two different load conditions according to the load direction applied on the nut. Therefore, the four installation modes of PRSM are (a) S-N-C, (b) S-N-T, (c) O-N-T and (d) O-N-C, where S represents the screw and nut supported at the same end while O represents that supported at opposite ends. N-C and N-T represent the compression or tension on the nut, respectively. The schematic diagram of the PRSM in different installation modes is shown in Fig. 1, where the threads are numbered from the fixed end to the free end of the screw.

The PRSM can transmit motion and force through the contacts of roller between screw and nut. As shown in Fig. 1, the axial load applied on the nut is first transmitted to the nut-roller interfaces, then to the screw-roller interfaces and finally to the fixed end of the screw. Before establishing the mathematical model, the following hypotheses need to be made: (1) the contact deformation is in the range of elastic deformation. (2) Only the axial load is permissible, the bending moment, tilting moment and radial load are prohibited [1]. (3) The load distribution and force states are the identical among all the rollers.

Then, according to the force equilibrium condition, the relationship between the axial load on each thread and the applied load F can be expressed as

$$\begin{cases} F = z\cdot\sum_{i=1}^{\tau} F_{SRi} \\ F = z\cdot\sum_{i=1}^{\tau} F_{NRi} \end{cases} \quad i = 1,2,\cdots,\tau \tag{1}$$

where F_{SRi} and F_{NRi} represent the axial load on the i^{th} thread couples of screw-roller and nut-roller interfaces, z and τ are the number and thread number of roller, respectively.

After the PRSM is loaded, the contact deformation will occur at the meshing point of the thread. Meanwhile, the shaft segment and thread of the screw, roller and nut are also deformed. Considering that there may be pitch errors in all threads, in this case, the deformation compatibility relationship in the i^{th} closed-loop formed by two adjacent contacting threads can be expressed as

$$\begin{cases} \sum \delta_{Si} + P_S = \sum \delta_{RSi} + P_R + e_{SRi} \\ \sum \delta_{Ni} + P_N = \sum \delta_{RNi} + P_R + e_{NRi} \end{cases} \tag{2}$$

where P_S, P_R and P_N represent the pitch of screw, roller and nut. $\Sigma\delta_{Si}$ and $\Sigma\delta_{RSi}$ are the sum of axial deformation of the screw and roller in the i^{th} closed-loop on the screw-roller interfaces, e_{SRi} is the sum of pitch error in this closed-loop. $\Sigma\delta_{Ni}$ and $\Sigma\delta_{RNi}$ represent the sum of axial deformation of the nut and roller, e_{NRi} is the sum of pitch error in the i^{th} closed-loop on the nut-roller interfaces. Generally, P_N, P_R and P_S are considered to be equal. However, the pitch deviation cannot be ignored because the difference between P_R and P_S (P_N) may be the same order of magnitude as the deviation of axial deformation.

According to the contact deformation, thread deformation and shaft segment deformation, the structural stiffness of PRSM can be discretized into contact stiffness, thread stiffness and shaft segment stiffness. Then, the Eq. (2) can be expressed by the corresponding structural stiffness and load of the thread [14]. Since there are a total of 2(τ-1) deformation compatibility relationships in the form of Eq. (2), combined with the force equilibrium condition given in Eq. (1), the matrix form equation of load distribution considering pitch deviation and pitch errors can be expressed as

$$\begin{cases} \mathbf{K}\cdot\mathbf{f} = \boldsymbol{\varepsilon} + \mathbf{e} \\ \left[\underbrace{1,1,\ldots,1}_{\tau},\underbrace{0,0,\ldots,0}_{\tau}\right]\cdot\mathbf{f} = F \Big/ z \\ \left[\underbrace{0,0,\ldots,0}_{\tau},\underbrace{1,1,\ldots,1}_{\tau}\right]\cdot\mathbf{f} = F \Big/ z \end{cases} \tag{3}$$

where $\mathbf{f} = [F_{NR1}, F_{NR2},\ldots, F_{NR\tau}, F_{SR1}, F_{SR2},\ldots, F_{SR\tau}]^{\mathrm{T}}$ is the vector of load distribution, $\mathbf{e} = [e_{NR1}, e_{NR2},\ldots, e_{NR\tau\text{-}1}, e_{SR1}, e_{SR2},\ldots, e_{SR\tau\text{-}1}]^{\mathrm{T}}$ is the vector of pitch errors. $\mathbf{K}$ is the stiffness matrix derived from the deformation compatibility relationship of all the closed-loops. According to the thread numbering rule, the axial load on the i^{th} shaft section of the nut supported at the same end is different from that of the nut supported at the opposite end, resulting in a different stiffness matrix. $\boldsymbol{\varepsilon}$ is the pitch deviation vector, which are opposite in the same installation configuration with different loading directions. As shown in Fig. 1, the contact thread surfaces are the same in installation mode S-N-C and O-N-T, then the pitch deviation vectors for the installation mode S-N-C and O-N-T are defined as

$$\boldsymbol{\varepsilon}_1 = \left[\underbrace{P_R - P_N, P_R - P_N,\ldots, P_R - P_N}_{\tau-1},\underbrace{P_R - P_S, P_R - P_S,\ldots, P_R - P_S}_{\tau-1}\right]^{T} \tag{4}$$

Similarly, the pitch deviation vectors for S-N-T and O-N-C are defined as

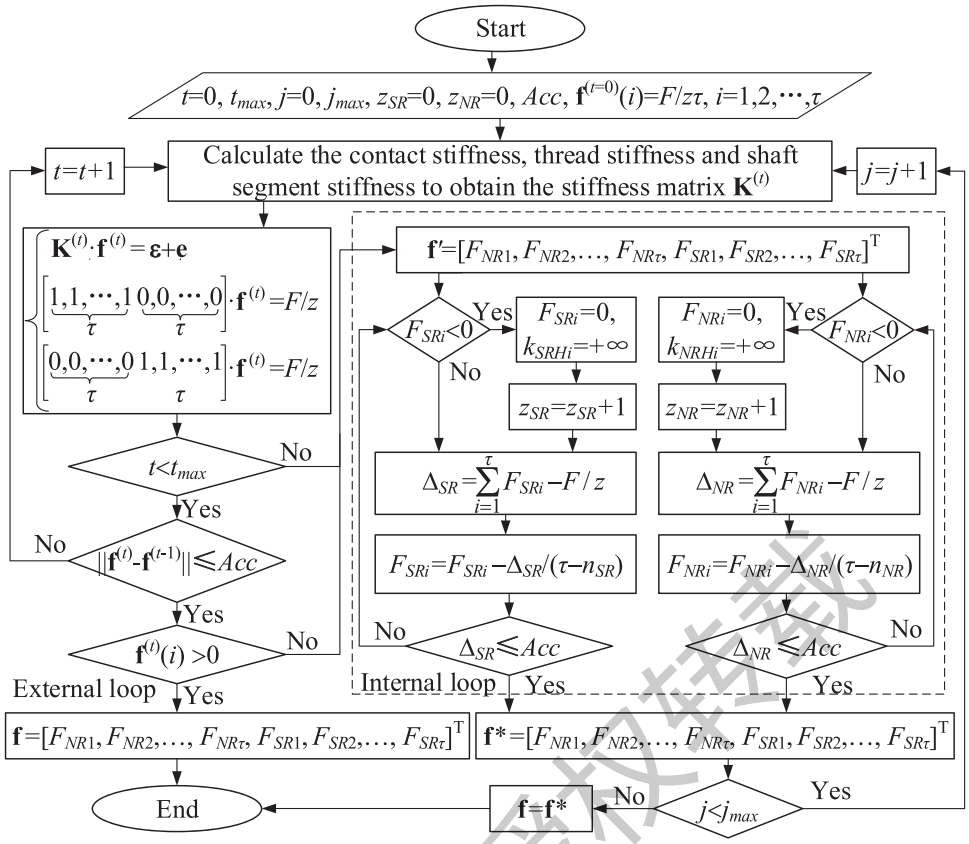

Fig. 2. Flow chart of the improved iterative algorithm for solving load distribution.

$$\varepsilon_2 = \left[\underbrace{P_N - P_R, P_N - P_R, \ldots, P_N - P_R}_{\tau-1}, \underbrace{P_S - P_R, P_S - P_R, \ldots, P_S - P_R}_{\tau-1}\right]^T \quad (5)$$

In order to reflect the non-uniform degree of load distribution, the load sharing coefficient is defined as the ratio of the load on each thread to the mean value, that is

$$\begin{cases} K_{SRi} = z\tau F_{SRi}/F \\ K_{NRi} = z\tau F_{NRi}/F \end{cases} \quad (6)$$

Moreover, the maximum load sharing coefficient $K_{SR} = \max(K_{SRi})$ and $K_{NR} = \max(K_{NRi})$ are important indexes that can directly reflect the non-uniformity of the load distribution in this study.

2.2. Improved iterative algorithm

An improved iterative algorithm is proposed to solve the load distribution of PRSM with pitch errors and pitch deviations, the flow chart is shown in Fig. 2.

Firstly, some parameters needed for the calculation are given as follows: the initial step $t = 0$ and the maximum number of iterations t_{max} for the external loop, the t and t_{max} are set as $j = 0$ and j_{max} for the internal loop. The initial number of unloaded thread on the screw-roller and nut-roller interfaces is $z_{SR} = z_{NR} = 0$. The convergence accuracy is Acc. All threads are assumed to be under the action of equal load in the initial step, *i.e.* the initial value of the load distribution is $\mathbf{f}^{(t=0)}(i) = F/z\tau$, $i = 1,2,\ldots,\tau$.

Then the contact stiffness, thread stiffness and shaft segment stiffness under the load distribution obtained in each step are calculated to form the stiffness matrix $\mathbf{K}^{(t)}$, which is then substituted into Eq. (3). The Eq. (3) will change in each step due to the nonlinearity of contact deformation until convergence. If $t < t_{max}$ is satisfied meanwhile there is no negative value in the results, the load distribution can be obtained just through the external loop, otherwise the internal loop is needed.

The function of the internal loop is to find whether there are unloaded threads and to make the load distribution meet the force equilibrium condition. The temporary load distribution **f'** obtained when jumping out of the external loop is served as the initial value for the internal loop. If $F_{SRi} < 0$, it means that the i^{th} couple of threads on the screw-roller interfaces are not loaded, so that $F_{Sri} = 0$, the contact stiffness is defined as infinite $k_{SRHi} = +\infty$ and the number of unloaded thread is recorded as $z_{SR} = z_{SR} + 1$. Then, $\Delta_{SR} = \sum_{i=1}^{\tau} F_{SRi} - F/z$, the load distribution is redistributed by $F_{SRi} = F_{SRi} - \Delta_{SR}/(\tau - z_{SR})$ until

Table 1
Structural parameters of PRSM.

Parameters (Unit)	Screw		Roller		Nut	
	Symbol	Value	Symbol	Value	Symbol	Value
Nominal diameter (mm)	d_{S0}	48	d_{R0}	16	d_{N0}	80
Major diameter (mm)	d_{S1}	49.43	d_{R1}	17.6	d_{N1}	82.62
Minor diameter (mm)	d_{S2}	45.38	d_{R2}	14	d_{N2}	78.57
Thread thickness (mm)	h_S	2	h_R	2.4	h_N	2
Pitch (mm)	P_S	5	P_R	5	P_N	5
Half of thread angle (°)	β_S	45	β_R	45	β_N	45
Starts of thread (Integer)	n_S	5	n_R	1	n_N	5
External diameter (mm)	/	/	/	/	d_{N3}	100
Thread number (Integer)	/	/	τ	20	/	/
Number of roller (Integer)	/	/	z	10	/	/

Table 2
Material parameters of PRSM.

Random variables (Unit)	Symbol	Value
Young's modulus (MPa)	E_S, E_R, E_N	212,000
Poisson's ratio (None)	ν_S, ν_R, ν_N	0.29
Yield limit (MPa)	σ_s	1617

$\Delta_{SR} \leq Acc$. For the nut-roller interfaces, the same operation is performed. If $j < j_{max}$, the load distribution $\mathbf{f}^*$ obtained in the internal loop will be returned to the external loop and then calculated again to meet the deformation compatibility relationship, otherwise $\mathbf{f}^*$ is the final result.

2.3. Numerical examples and analysis

In order to reveal the effect of pitch errors and the pitch deviations on

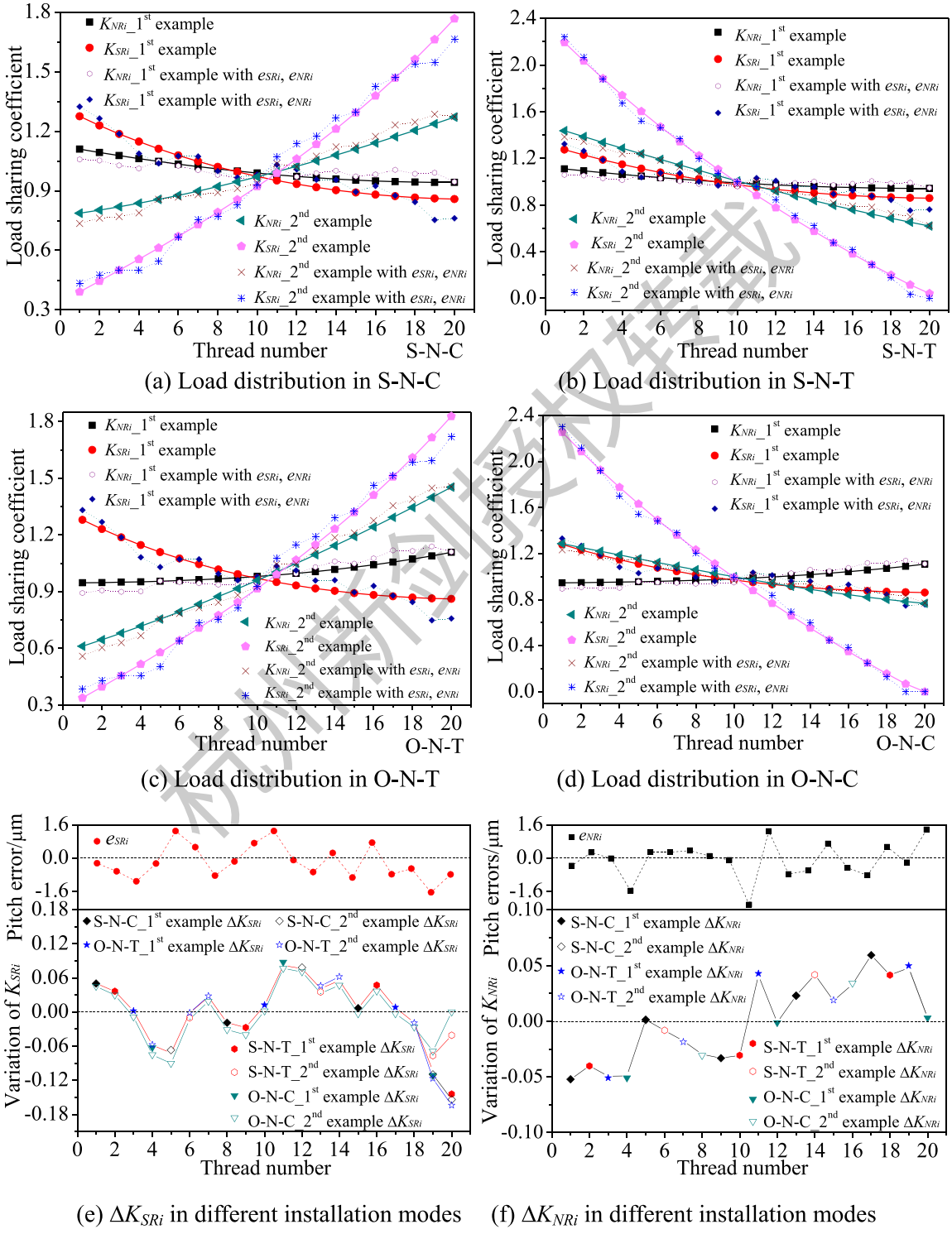

Fig. 3. Comparison of load distribution under the effect of pitch deviation and pitch errors, (a) Load distribution in S-N-C, (b) Load distribution in S-N-T, (c) Load distribution in O-N-T, (d) Load distribution in O-N-C, (e) ΔK_{SRi} in different installation modes, (f) ΔK_{NRi} in different installation modes.

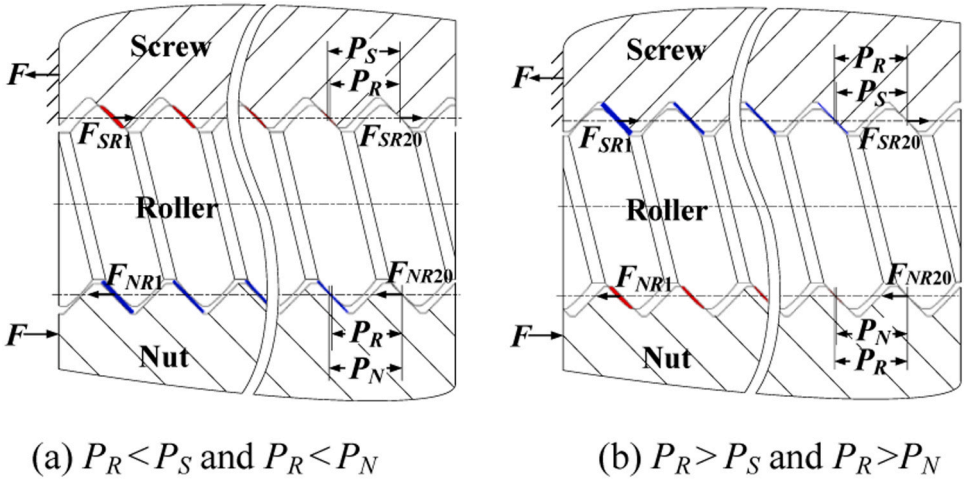

Fig. 4. Effect of pitch deviation on installation mode S-N-C, (a) $P_R < P_S$ and $P_R < P_N$, (b) $P_R > P_S$ and $P_R > P_N$.

the load distribution of PRSM, the numerical examples for different installation modes will be conducted with the structural parameters given in Table 1. The material is GCr15 [23], a kind of rolling bearing steel with good abrasion resistance and superior contact fatigue performance, and its material parameters are shown in Table 2 [4]. The manufacturing precision of PRSM is G5 according to the ISO 3408–3 [1] and the error within 0.25 μm is permitted for each pitch [5].

2.3.1. Effect of pitch errors

Based on the parameters given in Tables 1 and 2, the PRSM without pitch deviation ($P_S = P_R = P_N = 5$) is taken as 1st example, and the PRSM with pitch deviation ($P_S = 4.999$, $P_R = 5.001$, $P_N = 5.002$) is taken as 2nd example. Then a group of random pitch errors of all the closed-loop are generated by MATLAB, which are normally distributed within ±0.25 μm and meets the 3σ criterion, as shown in Fig. 3. Then, a series of numerical examples are carried out to calculate the load distribution of PRSM in the four installation modes by the improved iterative algorithm, including 1st and 2nd example without pitch errors, 1st and 2nd example with pitch errors. 60 kN is selected here as an example of axial load.

The comparison of load distribution under the effect of pitch deviations and pitch errors is shown in Fig. 3. As shown in Fig. 3(a) and (b), the load distribution of 1st example in the S-N-C and S-N-T is basically the same, that is, the load decreases with the thread number on both screw-roller and nut-roller interfaces. Similarly, Fig. 3(c) and 3(d) show that the load distribution of the 1st example in O-N-T and O-N-C is almost the same, the load decreases with the thread number on the screw-roller interfaces while increases with the thread number on the nut-roller interfaces. In conclusion, in any installation modes without pitch deviations and pitch errors, the load is the largest at the fixed end of the screw or the loading end of the nut while the load is smallest at their free ends.

For 2nd example, the load distributions in the four installation modes are considerably affected and become more non-uniform on both screw-roller and nut-roller interfaces. Fig. 3(a) shows that the load distribution trend of 2nd example in S-N-C is completely reversed, and the load increases with the thread number on both sides. Fig. 3(b) depicts the uniformity of load distribution of 2nd example in S-N-T deteriorates more seriously and the last thread couple on screw-roller interfaces are not even loaded. From Fig. 3(c), it can be seen that the load distribution trend of 2nd example in O-N-T is the similar to that of S-N-C, but the uniformity of O-N-T is much worse. As shown in Fig. 3(d), the load distribution trend of 2nd example in O-N-C is the similar to that of S-N-T, but the load distribution on the nut-roller interfaces is obviously more uniform than that of O-N-C.

Moreover, the screw-roller interfaces is more severely affected by the pitch deviation, and the load distribution on the nut-roller interface is more uniform. This is mainly because the pitch deviation between screw and roller (2 μm) is larger than that between nut and roller (1 μm), and the shaft stiffness of nut is also greater than that of screw in these

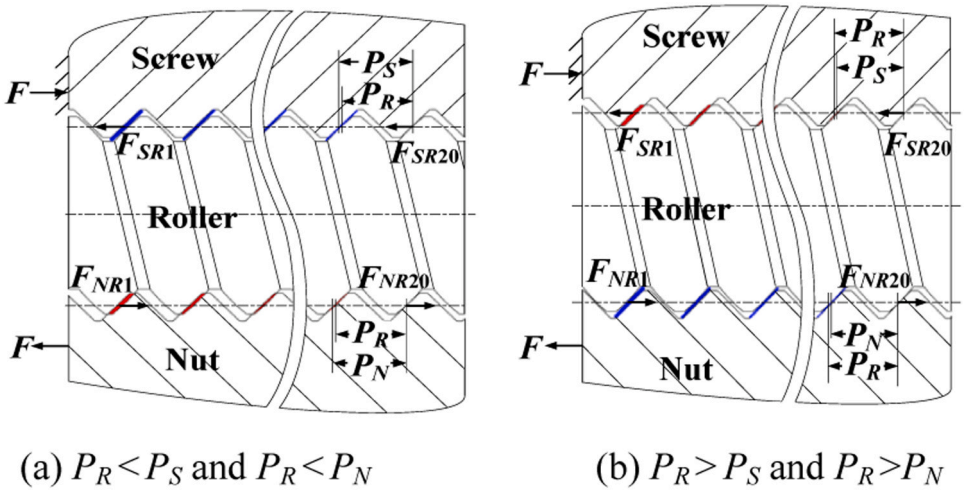

Fig. 5. Effect of pitch deviations on installation mode S-N-T, (a) $P_R < P_S$ and $P_R < P_N$, (b) $P_R > P_S$ and $P_R > P_N$.

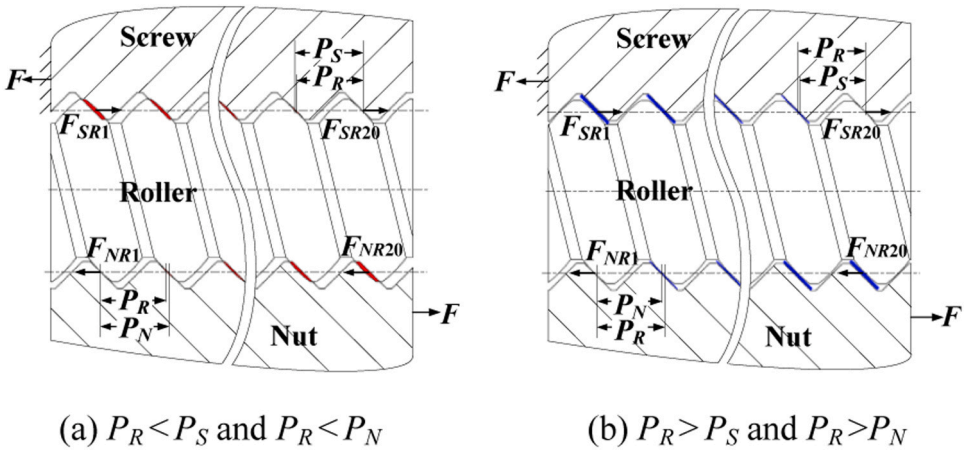

Fig. 6. Effect of pitch deviations on installation mode O-N-T, (a) $P_R < P_S$ and $P_R < P_N$, (b) $P_R > P_S$ and $P_R > P_N$.

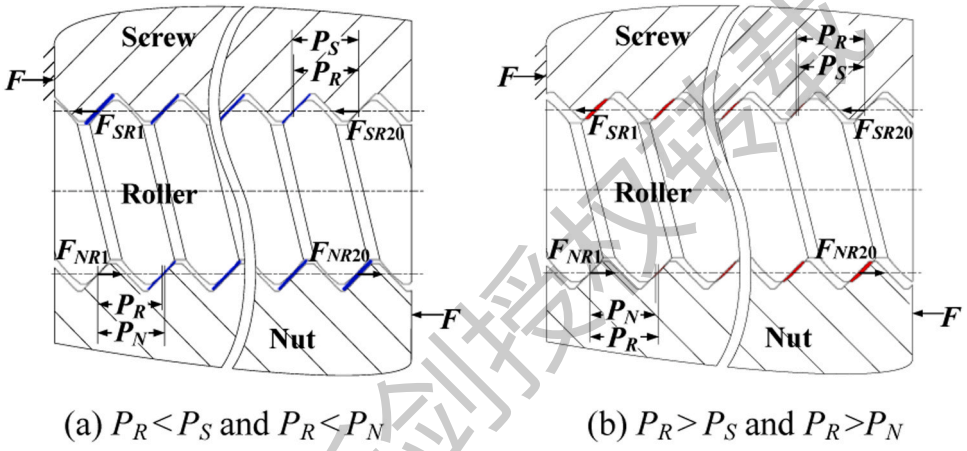

Fig. 7. Effect of pitch deviations on installation mode O-N-C, (a) $P_R < P_S$ and $P_R < P_N$, (b) $P_R > P_S$ and $P_R > P_N$.

examples.

Compared with the1st example, the load distribution of the 2nd example is fluctuant under the influence of pitch errors, and the load sharing coefficient variations of the i^{th} thread couples on the screw-roller and nut-roller interfaces are represented by ΔK_{SRi} and ΔK_{NRi}. The relationships between pitch errors and ΔK_{SRi}, ΔK_{NRi} is shown in Fig. 3(e) and (f), and some overlapping points are not shown. It can be found that the influence of the same pitch error on 1st and 2nd example in the four installation modes is basically the same, except for the case of unloaded threads, such as the 20th thread of the 2nd example in S-N-T and O-N-C. This is because in any installation mode of the 1st or 2nd example, each random pitch error is applied to the closed-loop independently only according to the thread number.

In general, the positive pitch error increases the clearance between the thread surfaces in contact, thereby compensating for the axial accumulative deformation and reducing the load on the thread. Conversely, the negative pitch error decreases the clearance, which can be assumed to apply a displacement on the thread couples, thus resulting in a larger load. Furthermore, all pitch errors have coupling and the cumulative effect on the load distribution. Therefore, the variation of load sharing coefficient is correlated with the variation trend of pitch error.

Table 3
Influence of pitch deviation on the load distribution.

Installation modes	Screw-roller interfaces		Nut-roller interfaces	
	$P_R < P_S$	$P_R > P_S$	$P_R < P_N$	$P_R > P_N$
S-N-C	w	c	c	w
S-N-T	c	w	w	c
O-N-T	w	c	w	c
O-N-C	c	w	c	w

2.3.2. *Effect of pitch deviation*

The above analysis shows that the load distribution of PRSM is mainly affected by the pitch deviation between roller and screw (nut). Moreover, the same pitch deviation has different effects on the four installation modes. In order to reveal these phenomena, the effect of pitch deviation on the load distribution in different installation modes of PRSM is studied through the structural analyses, as shown in Figs. 4–7. The clearance decreasing between the contacting threads is marked in red while clearance increasing is marked in blue. Besides, the thickness reflects the value of the clearance decreasing or increasing.

The force analysis of S-N-C with $P_R < P_S$ and $P_R < P_N$ is taken as an example, as shown in Fig. 4(a). On the screw-roller interfaces, the clearance decreases gradually from the free end to the fix end of the screw. Consequently, compared with the PRSM without pitch deviation, the original maximum load on the thread near the fixed end becomes larger. To maintain the force equilibrium condition, the original minimum load on the free end of the screw becomes smaller. In this case, the load distribution trend remains unchanged, but the gradient is higher, that is, the load distribution uniformity is getting worse, which is indicated by the symbol "w". On the nut-roller interfaces, the clearance increases gradually from the free end to the loading end of the nut. As a

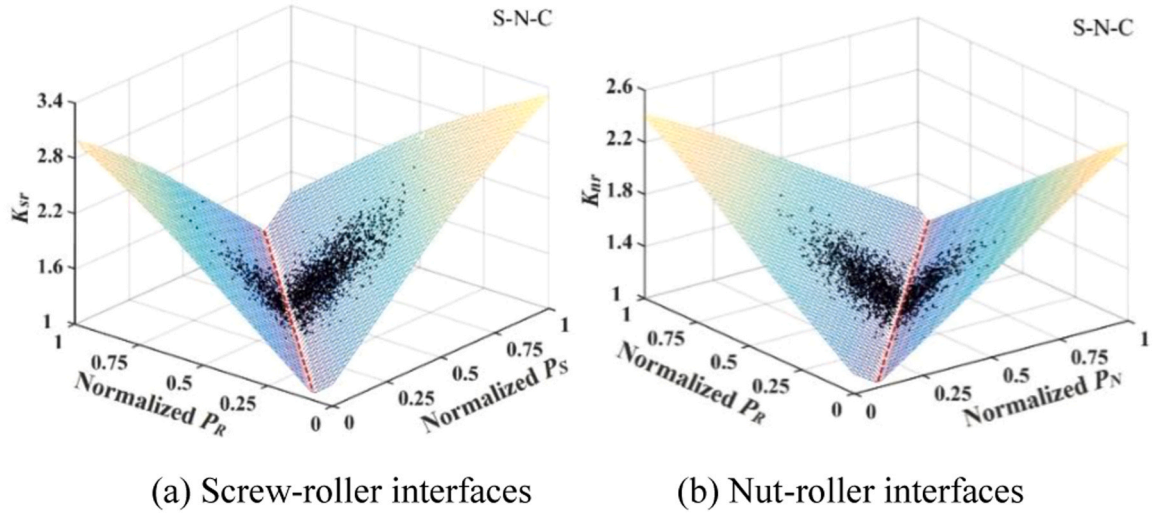

Fig. 8. 3D grid surface diagrams in S-N-C, (a) Screw-roller interfaces, (b) Nut-roller interfaces.

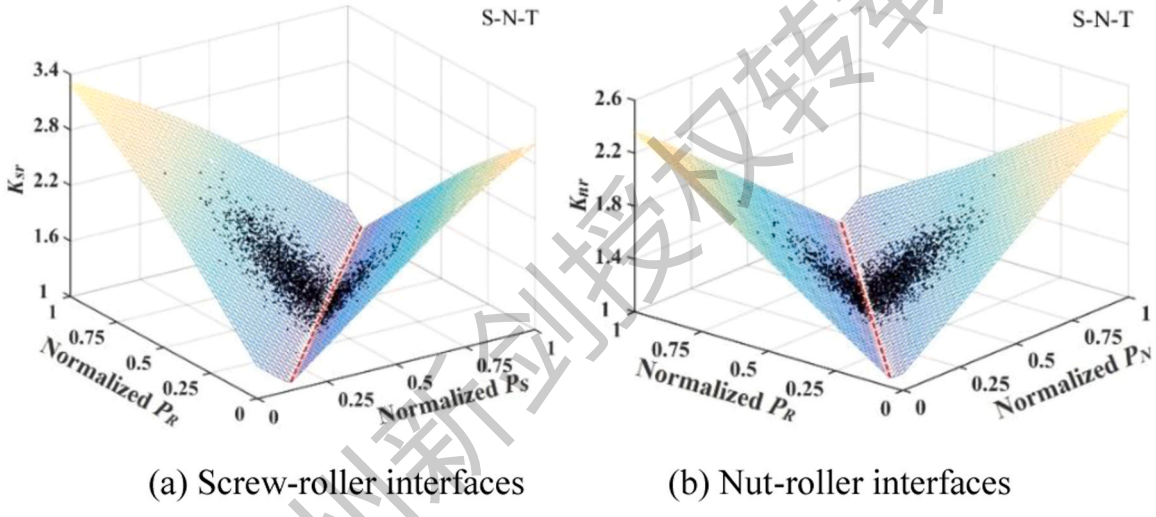

Fig. 9. 3D grid surface diagrams in S-N-T, (a) Screw-roller interfaces, (b) Nut-roller interfaces.

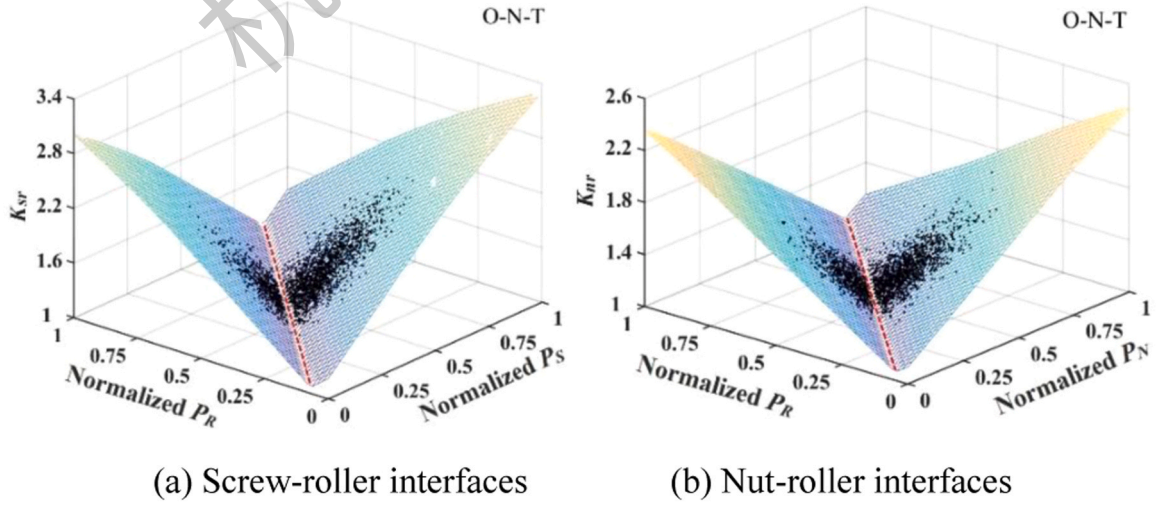

Fig. 10. 3D grid surface diagrams in O-N-T, (a) Screw-roller interfaces, (b) Nut-roller interfaces.

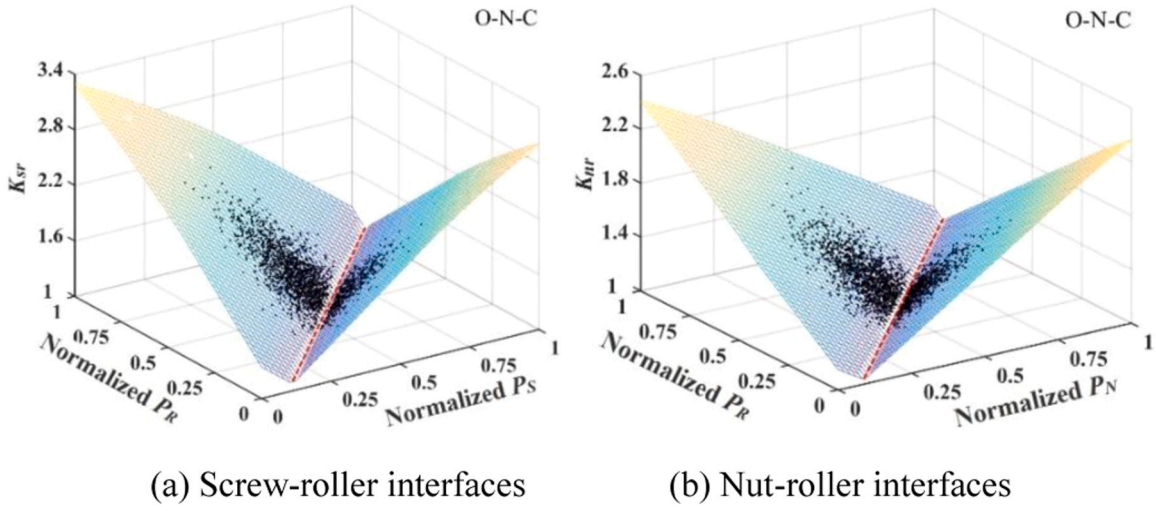

(a) Screw-roller interfaces (b) Nut-roller interfaces

Fig. 11. 3D grid surface diagrams in O-N-C, (a) Screw-roller interfaces, (b) Nut-roller interfaces.

result, compared with the PRSM without pitch deviation, the original maximum load on the thread near the loading end decreases, while the original minimum load on the free end of the nut increases accordingly. Thus, this effect is defined as a change in load distribution trend and is represented by the symbol "c". Similarly, all the analysis results of Figs. 4–7 are shown in Table 3.

In order to visually display the relationship between the pitch deviation and load distribution in different installation modes, the 3D grid surface diagrams of the normalized pitch and the maximum load sharing coefficient formed by 2500 random samples are shown in Figs. 8–11. These figures clearly show that the load distribution on the screw-roller interface is more likely to be non-uniform than that on the nut-roller interface under the influence of pitch deviation.

As shown by the red lines in Figs. 8–11, there are valley structure regions with minimum values of K_{SR} and K_{NR} on both screw-roller and nut-roller interfaces, indicating more uniform load distribution can be obtained by optimizing. On the screw-roller interfaces, the grid surfaces with the same load directions of the screw are similar. For S-N-C and O-N-T, the line is in the region of $P_R > P_S$ when the screw is under tension. For S-N-T and O-N-C, the line is in the region of $P_R < P_S$ when the screw is under compression. On the nut-roller interfaces, the grid surfaces with the same load directions of the nut are similar. When the nut is under compression, the line is in the region of $P_R < P_N$ for S-N-C and O-N-C, while in the region of $P_R > P_N$ for S-N-T and O-N-T when the nut is under tension.

In addition, it can be found that these valleys are located in the region of where the load distribution trend changes in Table 3, and there are significantly more sample points on the other side of the valley. Furthermore, in this region, the appropriate pitch deviation between P_R and P_S (or P_N) can improve the load distribution uniformity, that is, K_{SR} (or K_{NR}) is smaller than the initial value. Conversely, the improper pitch deviation will not only reverse the load distribution trend but also increase the non-uniformity of load distribution.

3. Multi-objective optimization on load distribution

3.1. Multi-objective optimization modelling

In order to improve the load carrying capacity of PRSM, the multi-objective optimization of the load distribution can be carried out for the different installation modes to help more effectively reach the valleys shown in Figs. 10–13. The pitches of the screw, roller and nut $\mathbf{P} = (P_S, P_R, P_N)^{\mathrm{T}}$ are selected as the design variables, and the other parameters are the design constants marked as $\mathbf{C_x} = (d_{S0}, d_{R0}, d_{N0}, \cdots, \beta_S, \beta_R, \beta_N)^{\mathrm{T}}$. Then, the maximum load sharing coefficient K_{SR} and K_{NR} are the function of $\mathbf{P}$ and $\mathbf{C_x}$, *i.e.* $K_{SR} = f_{SR}(\mathbf{P}, \mathbf{C_x})$ and $K_{NR} = f_{NR}(\mathbf{P}, \mathbf{C_x})$. And the constraint conditions are given to ensure that threads do not interfere. Therefore, the multi-objective optimization model can be expressed as

$$\begin{aligned} &find && P = (P_S, P_R, P_N)^T \\ &\min && f_{SR}(P, C_x)\,\&f_{NR}(P, C_x) \\ &s.t. && \begin{cases} |P_S - P_R| - \dfrac{\min(P_R, P_S) - h_S - h_R}{\tau - 1} < 0 \\ |P_N - P_R| - \dfrac{\min(P_R, P_N) - h_N - h_R}{\tau - 1} < 0 \\ P^l \le P \le P^u \end{cases} \end{aligned} \tag{7}$$

where $\mathbf{P}^l$ and $\mathbf{P}^u$ are the lower and upper bound of the design space. In this case, the optimal design of $\mathbf{P}$ is searched for the minimum values of objective function.

3.2. NSGA-II algorithm

The flow chart of the multi-objective optimization on load distribution for PRSM base on NSGA-II algorithm [22] is shown in Fig. 12, and the steps are as follows:

Step 1 Set the maximum generation and the population size as t_{max} and S.

Step 2 Generate the initial population M_t (t = 0) randomly.

Step 3 Calculate the optimization objectives $f_{SR}(\mathbf{P}, \mathbf{C_x})$ and $f_{NR}(\mathbf{P}, \mathbf{C_x})$ of M_t.

Step 4 Implement the non-dominated sorting for M_t based on the dominance relation in the objective space. Then, the crowding distance is assigned as follows:

(1) Initialize the distance of all the individuals to 0, *i.e.* $D(i) = 0$;
(2) Sort the individuals in ascending order;
(3) Assign the infinite distance to boundary values for each individual, *i.e.* $D(1) = \infty$ and $D(S) = \infty$;
(4) The crowding distance for the i^{th} individual sorted in the middle can be expressed as

$$D(i) = D(i) + \frac{f(i) - f(i-1)}{f^{\max} - f^{\min}} \tag{8}$$

where $f(*)$ is the value of objective function, f^{max} and f^{min} are the maximum and minimum value, respectively.

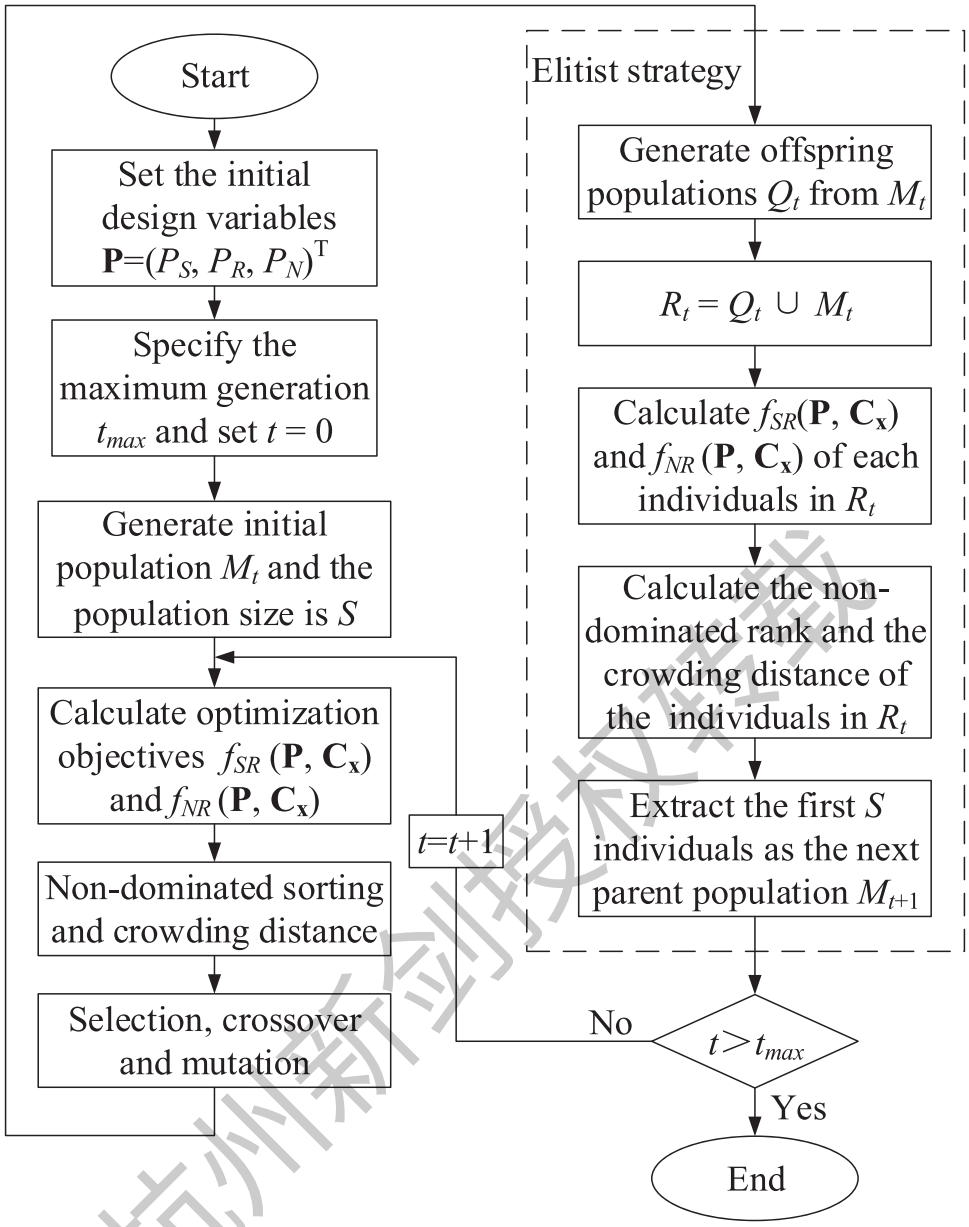

Fig. 12. Flow chart of multi-objective optimization base on NSGA-II algorithm.

Step 5 Perform the selection by using a crowded comparison operator. Based on simulated binary crossover method, the crossover operation is performed as follows :

$$P_i^{(1,t+1)} = \frac{1+\beta_\chi}{2}P_i^{(1,t)} + \frac{1-\beta_\chi}{2}P_i^{(2,t)}$$
$$P_i^{(2,t+1)} = \frac{1-\beta_\chi}{2}P_i^{(1,t)} + \frac{1+\beta_\chi}{2}P_i^{(2,t)} \quad (9)$$

where $P_i^{(j,t+1)}$ is the j^{th} offspring of the t^{th} generation for the i^{th} design variable. β_χ (≥ 0) is a sample generated from a random number with the density.

The mutation operation can be performed as:

$$P_i^{(1,t+1)} = P_i^{(1,t)} + \alpha_\varsigma\left(P_i^u - P_i^l\right)$$
$$\alpha_\varsigma = \begin{cases} (2r_\varsigma)^{\frac{1}{\eta_m+1}} - 1\ , & r_\varsigma < 0.5 \\ 1 - [2(1-r_\varsigma)]^{\frac{1}{\eta_m+1}}, & r_\varsigma \geq 0.5 \end{cases} \quad (10)$$

where α_ς is a small variation, r_ς is an uniformly sampled random number and $r_\varsigma \in [0,1]$, η_m is the coefficient of mutation distribution.

Step 6 After the offspring population Q_t is generated from step 5, the temporary population R_t is created by combining offspring population Q_t and the current generation population M_t.

Step 7 Calculate the non-dominated rank and the crowding distance of the individuals in R_t.

Step 8 Extract the first S individuals from R_t as the next parent population M_{t+1}. Therefore, the elitism can be ensured as the best individuals of the previous and current population are added to the next

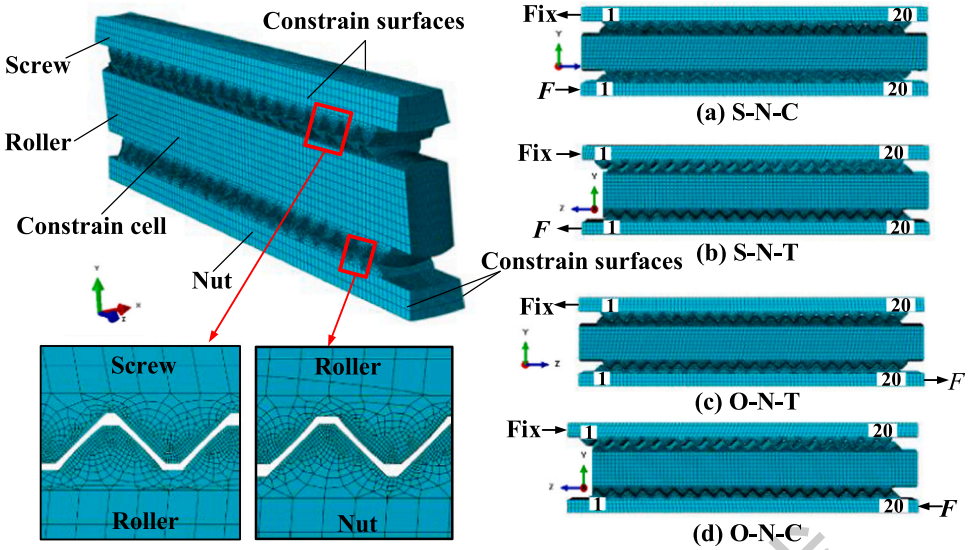

Fig. 13. FE model of PRSM for different installation modes.

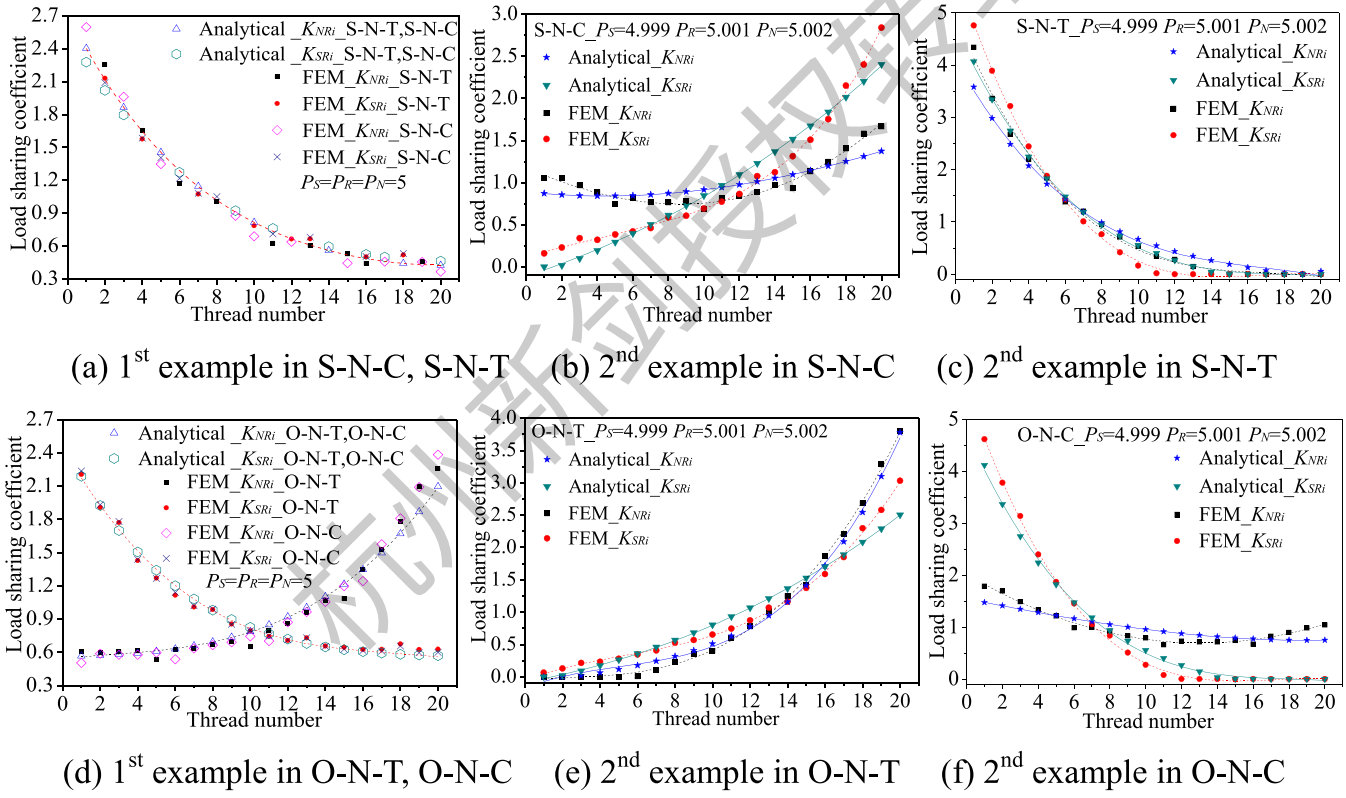

Fig. 14. Comparison of load distribution obtained by analytical method and FEM, (a) 1st example in S-N-C, S-N-T, (b) 2nd example in S-N-C, (c) 2nd example in S-N-T, (d) 1st example in O-N-T, O-N-C, (e) 2nd example in O-N-T, (f) 2nd example in O-N-C 4.2.

population.

Step 9 Repeat the step 3–8 to generate the subsequent generations until $t > t_{max}$.

4. Results and discussion

4.1. Mathematical model verification

To verify the correctness of the mathematical model of load distribution considering pitch deviation, the finite element (FE) models of PRSM corresponding to the numerical examples are established in ABAQUS software. As shown in Fig. 13, the FE model only contains one roller and the parts are simplified to reduce the calculation cost and pursue better pursue convergence. The thread surface is refined to improve the calculation accuracy. After the mesh independence test, the global and local mesh seed size of the FE models are 1.2 mm and 0.12 mm, including 1,499,718 linear hexahedral elements of type C3D8R and 58,970 linear wedge elements of type C3D6.

In Fig. 13, the screw and nut are symmetrically constrained on the two sides while the roller is constrained on the cell body, and only the

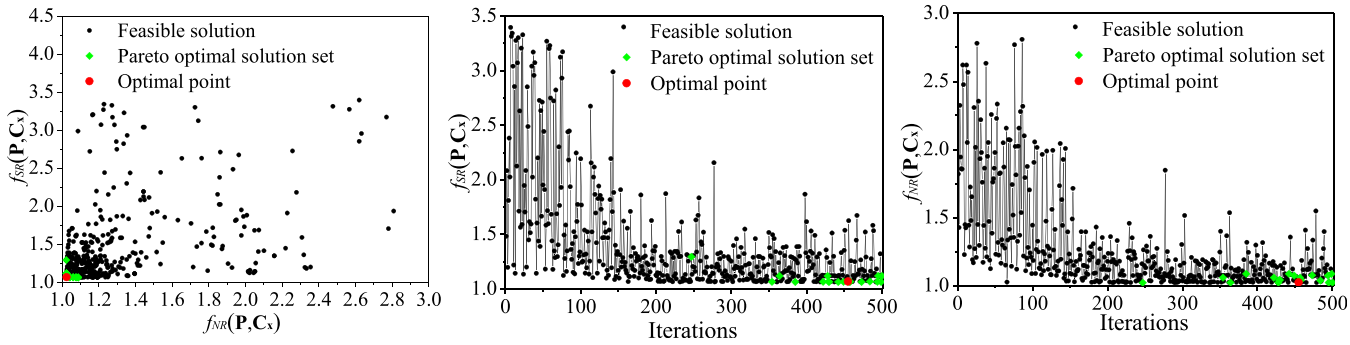

(a) Scatter of $f_{SR}(\mathbf{P},\mathbf{C_x})$ and $f_{NR}(\mathbf{P},\mathbf{C_x})$ (b) History graph of $f_{SR}(\mathbf{P},\mathbf{C_x})$ (c) History graph of $f_{NR}(\mathbf{P},\mathbf{C_x})$

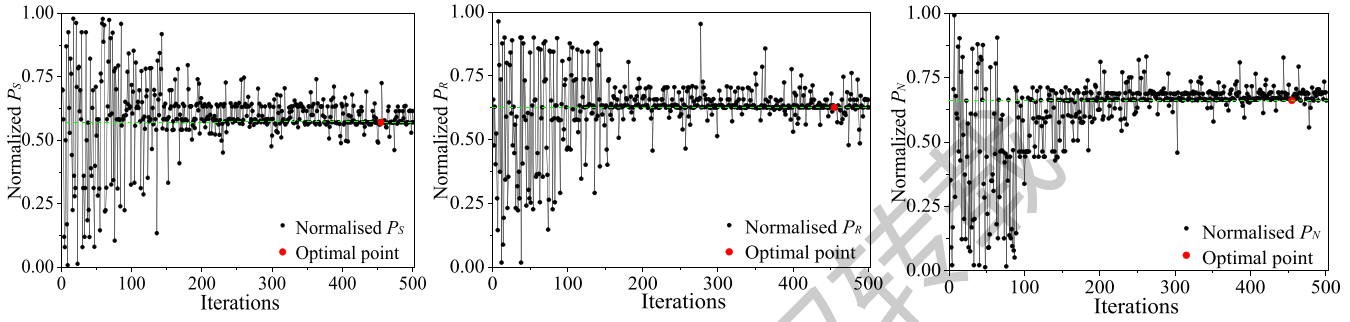

(d) History graph of P_S (e) History graph of P_R (f) History graph of P_N

Fig. 15. Optimization history graphs of installation mode S-N-C, (a) Scatter of $f_{SR}(\mathbf{P},\mathbf{C_x})$ and $f_{NR}(\mathbf{P},\mathbf{C_x})$, (b) History graph of $f_{SR}(\mathbf{P},\mathbf{C_x})$, (c) History graph of $f_{NR}(\mathbf{P},\mathbf{C_x})$, (d) History graph of P_S, (e) History graph of P_R, (f) History graph of P_N.

freedom degree of axial displacement is released. The interaction and boundary condition are varied according to the different installation modes. A small displacement is applied to establish the contact relationship smoothly in the first step due to the existence of clearance and then replaced by the axial load in the second step.

Corresponding to the cross-sectional areas of the screw, roller and nut in the simplified FE models, the load distributions of the numerical examples under 3 kN are calculated by analytical and FEM method, as shown in Fig. 14. The results show that the load distribution curves obtained by analytical method and FEM are basically consistent, and the improved iterative algorithm can effectively and accurately calculate the load distribution with no-load threads. Additional calculations show that the relative errors obtained by the two methods are also within the acceptable range if the axial load is changed. Besides, by comparing the 1st and 2nd example, it can be found that the pitch deviation affects the load distribution as the way summarized in Table 3. Therefore, the mathematical model proposed in this paper is correct through verification.

4.2. Optimization results discussion

The verified mathematical model of PRSM is further applied to the multi-objective optimization on load distribution by MATLAB. The applied load here is 60 kN, which can be designed according to the customer's requirements in practical application. Based on NSGA-II algorithm, the maximum generation and the population size are $t_{max} = 25$ and $S = 20$, then the optimization history graphs of the installation mode S-N-C are shown in Fig. 15.

There are 19 Pareto optimal solutions in 501 iterations, among which the optimal point can achieve the minimum value of $f_{SR}(\mathbf{P}, \mathbf{C_x})$ and

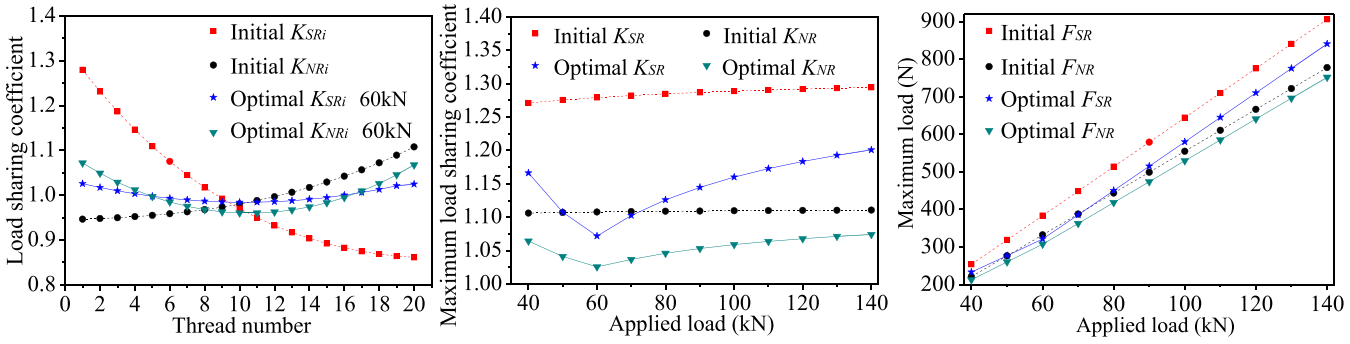

(a) Load distribution under 60 kN (b) Maximum load sharing coefficient (c) Maximum load

Fig. 16. Comparison of load carrying capacity between the initial and optimal PRSM, (a) Load distribution under 60 kN, (b) Maximum load sharing coefficient, (c) Maximum load.

Table 4
Optimal results of different installation modes.

	S-N-C	S-N-T	O-N-T	O-N-C
Initial P_S,P_R, P_N	0.5	0.5	0.5	0.5
Initial f_{SR}(**P**, $\mathbf{C_x}$)	1.27	1.27	1.28	1.28
Initial f_{NR}(**P**, $\mathbf{C_x}$)	1.11	1.11	1.11	1.11
Optimal P_S	0.57	0.56	0.55	0.64
Optimal P_R	0.62	0.51	0.61	0.59
Optimal P_N	0.66	0.47	0.58	0.62
Optimal f_{NR}(**P**, $\mathbf{C_x}$)	1.02	1.02	1.02	1.02
Optimal f_{SR}(**P**, $\mathbf{C_x}$)	1.07	1.07	1.07	1.07

f_{NR}(**P**, $\mathbf{C_x}$). While f_{NR}(**P**, $\mathbf{C_x}$) is smaller than f_{SR}(**P**, $\mathbf{C_x}$), indicating that more uniform load distribution can be achieved on the nut-roller interfaces. From the history curve of normalized P_S, P_R and P_N, the optimal point appears in the 455 iterations, which satisfies $P_S < P_R < P_N$ and is located in the valley region shown in Fig. 8.

Fig. 16 shows the comparison of load carrying capacity between the initial and optimal PRSM. Fig. 16(a) depicts that the minimum load is on the middle thread and the load distribution on both sides of the roller is significantly more uniform after optimization. As shown in Fig. 16(b), within the common operating load range [1], the maximum load sharing coefficient of the initial PRSM basically remains unchanged, while that of the optimal PRSM decreases obviously, especially reaching the

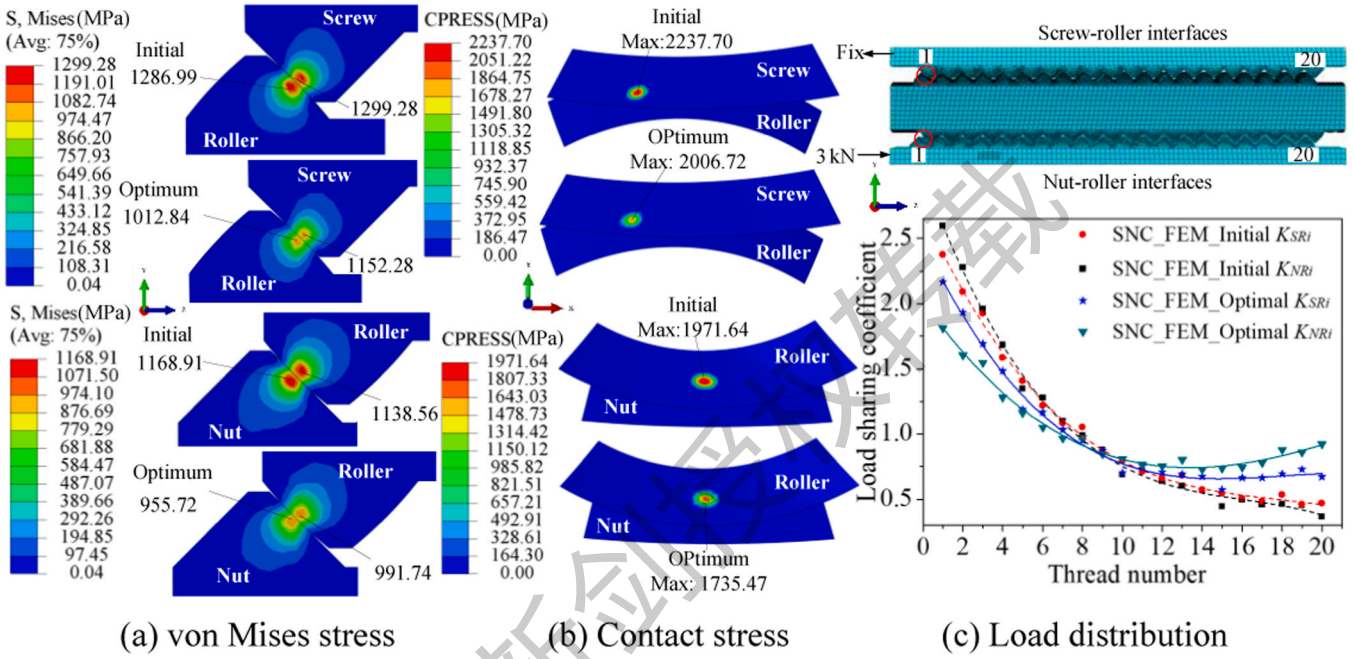

Fig. 17. Comparison between initial and optimized PRSM of S-N-C by FEM, (a) von Mises stress, (b) Contact stress, (c) Load distribution.

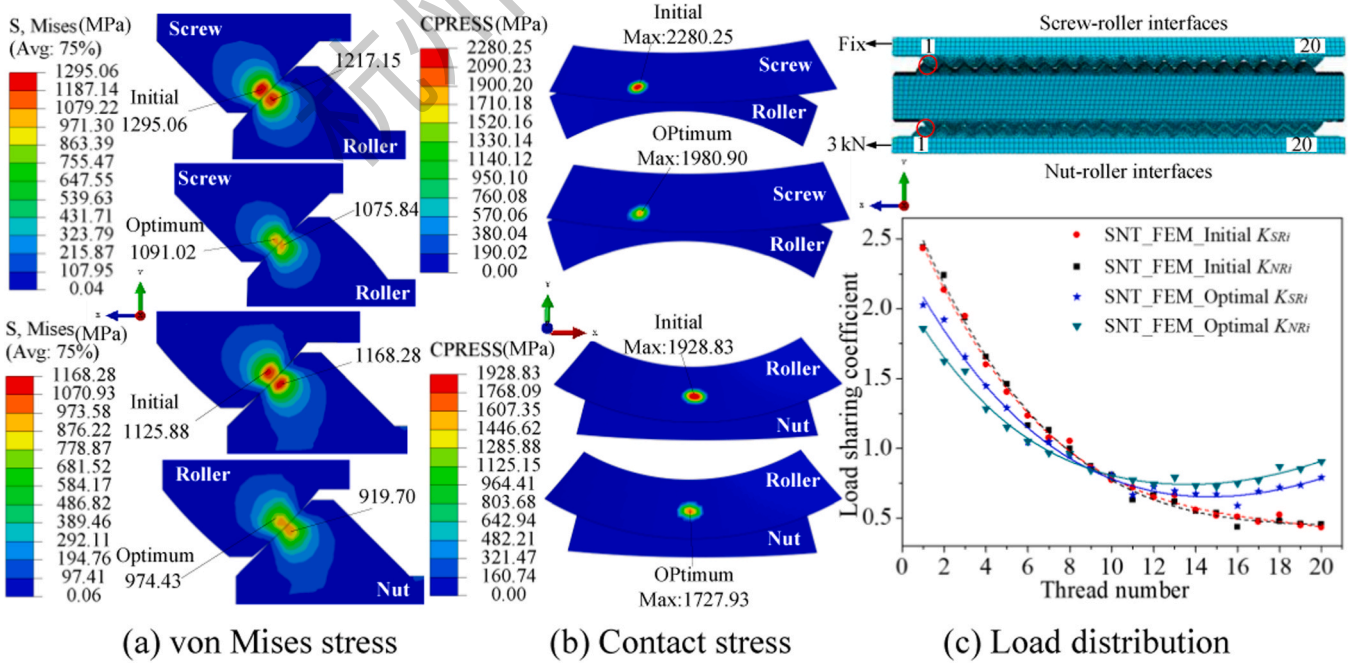

Fig. 18. Comparison between initial and optimized PRSM of S-N-T by FEM, (a) von Mises stress, (b) Contact stress, (c) Load distribution.

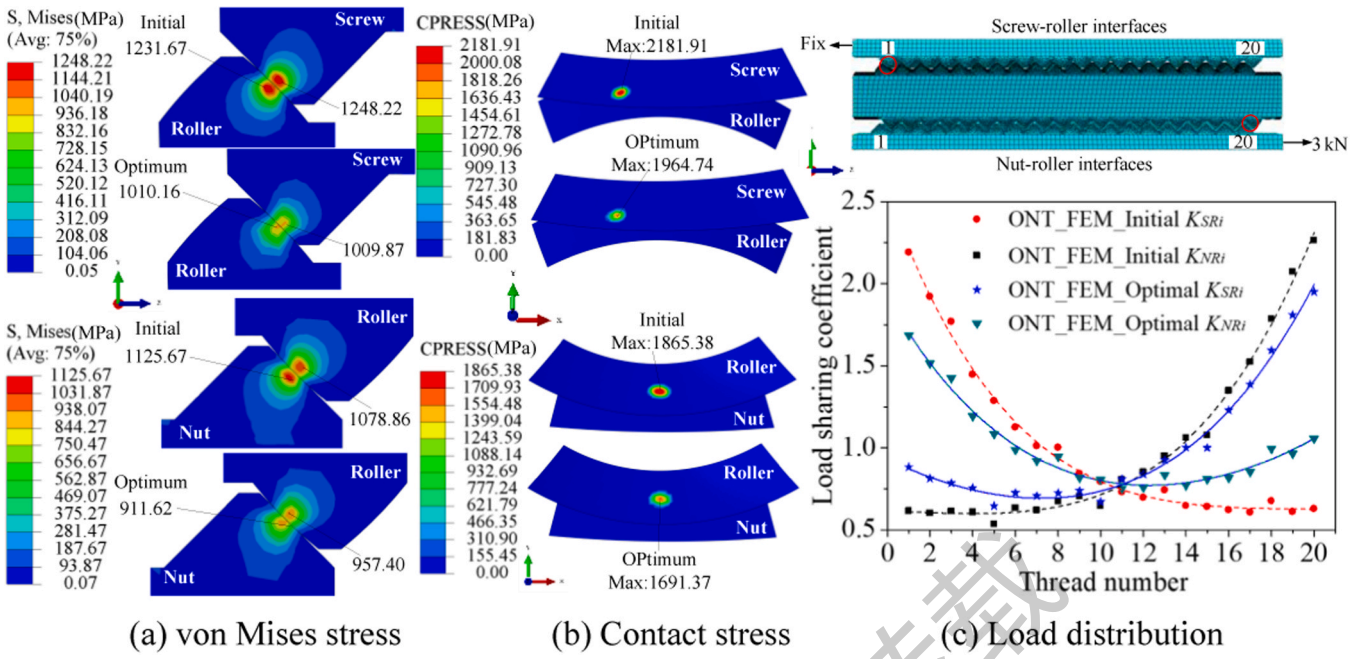

Fig. 19. Comparison between initial and optimized PRSM of O-N-T by FEM, (a) von Mises stress, (b) Contact stress, (c) Load distribution.

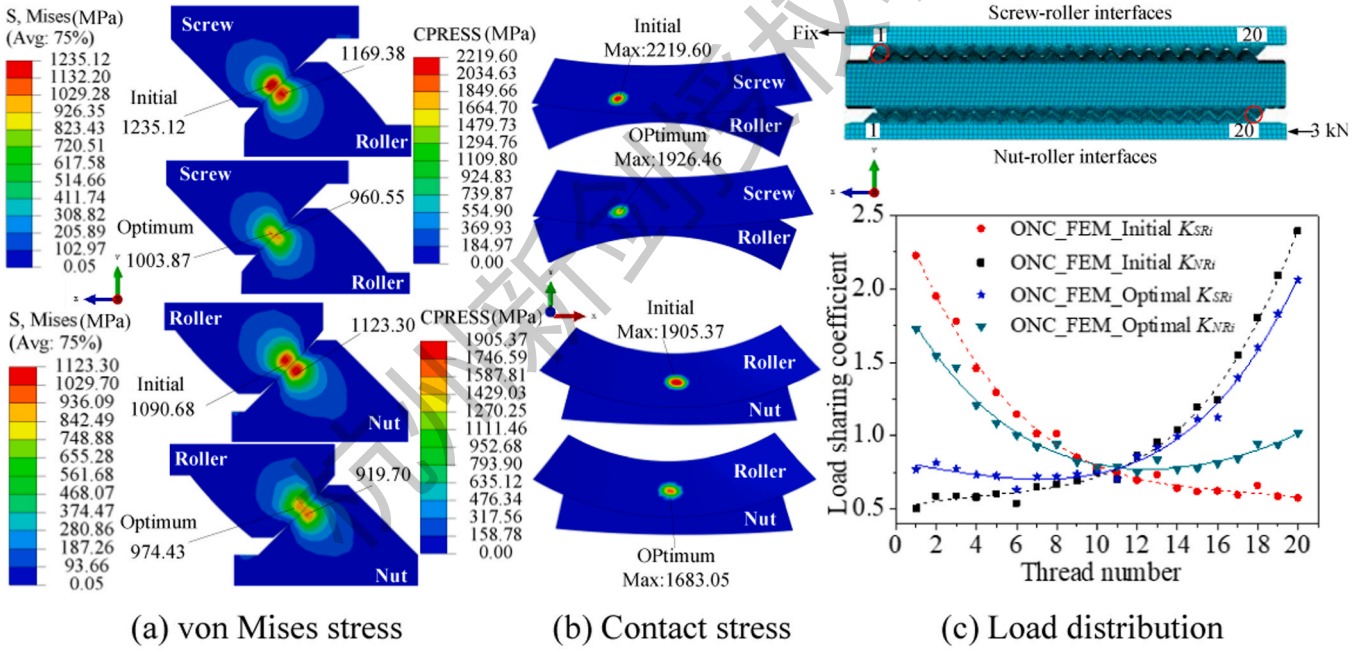

Fig. 20. Comparison between initial and optimized PRSM of O-N-C by FEM, (a) von Mises stress, (b) Contact stress, (c) Load distribution.

minimum value under the designed load. Fig. 16(c) shows that the maximum load on the thread of the optimal PRSM is also reduced for the same applied load. In conclusion, the load carrying capacity of optimal PRSM has been improved.

Similarly, the multi-objective optimization is performed for other installation modes, and the results are shown in Table 4.

The comparison between the initial and optimization results in different installation modes are displayed by FEM, as shown in Figs. 17–20. The results showed that the maximum load, von Mises stress and contact stress and decreased significantly after optimization. The load on thread close to the fixed end of the screw and the loading end of the nut decreases, while that of the other end increases, and the minimum load appears in the middle thread. Moreover, the standard deviation of load sharing coefficient for the installation mode S-N-C, S-N-T, O-N-T and O-N-C have been reduced by 22.44%, 22.71%, 17.35% and 17.82%. Therefore, FEM verification shows that the load distribution uniformity is improved, which can also be used to validate other applied loads.

5. Conclusions

In this paper, the mathematical model of PRSM is established to obtain the load distribution of planetary roller screw mechanism (PRSM) in different installation modes considering pitch errors and pitch deviation. An improved iterative algorithm is proposed to solve the calculation un-convergence caused by unloaded thread. Then, the multi-

objective optimization based on non-dominated sorting genetic algorithm (NSGA-II) is conducted to achieve a more uniform load distribution on both the screw-roller and nut-roller interfaces. Main conclusions are drawn as follows:

(1) The load distribution of PRSM is mainly affected by the pitch deviation between roller and screw (nut), which has a more serious impact on the screw-roller interfaces and has varying effects on different installation methods. Under the coupling and cumulative effects of pitch errors, the load distribution will fluctuate compared with the previous one without pitch errors, and the influence of pitch errors on the four installation modes is basically the same whether there is pitch deviation or not.
(2) There is a valley region with the most uniform load distribution on the 3D grid surface diagrams of the pitch and the maximum load sharing coefficient. On the screw-roller interfaces, the valley is in the region of $P_R > P_S$ for S-N-C and O-N-T, while in the region of $P_R < P_S$ for S-N-T and O-N-C. On the nut-roller interfaces, the valley is in the region of $P_R < P_N$ for S-N-C and O-N-C, while in the region of $P_R > P_N$ for S-N-T and O-N-T.
(3) After optimization, the load distribution is significantly more uniform on both sides of the roller, and the load carrying capacity of PRSM is improved effectively, which is verified by the FEM.

CRediT authorship contribution statement

Qin Yao: Writing - Original draft preparation, Conceptualization, Software, Validation. **Mengchuang Zhang:** Methodology, Reviewing and Editing. **Yongshou Liu:** Supervision. **Shangjun Ma:** Reviewing and Editing.

Declaration of Competing Interest

The authors declare that they have no known competing financial interests or personal relationships that could have appeared to influence the work reported in this paper.

Acknowledgments

This work was supported in part by the National Natural Science Foundation of China (grand no. 51875458), Industrial Development and Foster Project of Yangtze River Delta Research Institute of NPU, Taicang (grand no. CY20210201).

References

[1] Satellite roller screws catalogue. LTK Lineartechnik Korb Gmbh. 2020, Germany. ⟨www.ltk.solidcomponents.com⟩.
[2] Qiao G, Liu G, Shi Z, Wang Y, Ma S, Lim TC. A review of electromechanical actuators for More/All Electric aircraft systems. P I Mech Eng C-J Mec 2017;232 (22):4128–51. https://doi.org/10.1177/0954406217749869.
[3] Arriola D, Thielecke F. Model-based design and experimental verification of a monitoring concept for an active-active electromechanical aileron actuation system. Mech Syst Signal Pr 2017;94:322–45. https://doi.org/10.1016/j.ymssp.2017.02.039.
[4] Yao Q, Liu Y, Zhang M, Liu G, Ma S. Investigation on the uncertain factors of the elastic–plastic contact characteristics of the planetary roller screw mechanism. P I Mech Eng C-J Mec 2019;233(5):1795–806. https://doi.org/10.1177/0954406218772607.
[5] Du X, Chen B, Zheng Z. Investigation on mechanical behavior of planetary roller screw mechanism with the effects of external loads and machining errors. Tribol Int 2021;154:106689. https://doi.org/10.1016/j.triboint.2020.106689.
[6] Xie Z, Xue Q, Wu J, Gu L, Wang L, Song B. Mixed-lubrication analysis of planetary roller screw. Tribol Int 2019;140:105883. https://doi.org/10.1016/j.triboint.2019.105883.
[7] Aurégan G, Fridrici V, Kapsa P, Rodrigues F. Wear behavior of martensitic stainless steel in rolling-sliding contact for planetary roller screw mechanism: study of the WC/C solution. Tribol Online 2016;11(2):209–17. https://doi.org/10.2474/trol.11.209.
[8] Aurégan G, Fridrici V, Kapsa P, Rodrigues F. Experimental simulation of rolling–sliding contact for application to planetary roller screw mechanism. Wear 2015;332–333:1176–84. https://doi.org/10.1016/j.wear.2015.01.047.
[9] Zhang W, Liu G, Ma S, Tong R. Load distribution over threads of planetary roller screw mechanism with pitch deviation. P I Mech Eng C-J Mec 2019;233(13): 4653–66. https://doi.org/10.1177/0954406218819575.
[10] Ma S, Liu G, Tong R, Fu X. A frictional heat model of planetary roller screw mechanism considering load distribution. Mech Base Des Struct 2015;43(2): 164–82. https://doi.org/10.1080/15397734.2014.938816.
[11] Mei X, Tsutsumi M, Tao T, Sun N. Study on the load distribution of ball screws with errors. Mech Mach Theory 2003;38(11):1257–69. https://doi.org/10.1016/S0094-114X(03)00070-3.
[12] Miller DL, Marshek KM, Naji MR. Determination of load distribution in a threaded connection. Mech Mach Theory 1983;18(6):421–30. https://doi.org/10.1016/0094-114X(83)90057-5.
[13] Jones MH, Velinsky SA. Contact kinematics in the roller screw mechanism. J Mech Des 2013;135(5). https://doi.org/10.1115/1.4023964.
[14] Zhang W, Liu G, Tong R, Ma S. Load distribution of planetary roller screw mechanism and its improvement approach. P I Mech Eng C-J Mec 2016;230(18): 3304–18. https://doi.org/10.1177/0954406215610361.
[15] Ryś J, Lisowski F. The computational model of the load distribution between elements in a planetary roller screw. J Theor Appl Mech 2014:52.
[16] Abevi F, Daidie A, Chaussumier M, Sartor M. Static load distribution and axial stiffness in a planetary roller screw mechanism. J Mech Des 2015;138(1):012301-1–012301-11. https://doi.org/10.1115/1.4031859.
[17] Zhdanov AV, Morozov VV. Theoretical study of the load distribution on the threads for roller screw mechanisms of a friction type. Procedia Eng 2016;150:992–9. https://doi.org/10.1016/j.proeng.2016.07.152.
[18] Lisowski F. The analysis of displacements and the load distribution between elements in a planetary roller screw. Applied mechanics and materials. Switzerland: Trans Tech Publ; 2014.
[19] Ma S, Zhang C, Zhang T, Liu G, Liu S. Thermo-mechanical coupling–based finite element analysis of the load distribution of planetary roller screw mechanism. Adv Mech Eng 2018;10(6). https://doi.org/10.1177/1687814018775254.
[20] Ma S, Liu G, Fu X, Zhang W, Qiao G. Load distribution of rollers considering errors in planetary roller screw mechanism. J Harbin Inst Technol 2015;47(7):98–102 [in Chinese).
[21] Lisowski F. The specific dynamic capacity of a planetary roller screw with random deviations of a thread pitch. J Theor Appl Mech 2017;55(3):991–1001. https://doi.org/10.15632/jtam-pl.55.3.991.
[22] Deb K, Pratap A, Agarwal S, Meyarivan T. A fast and elitist multiobjective genetic algorithm: NSGA-II. IEEE Trans Evol Comput 2002;6(2):182–97. https://doi.org/10.1109/4235.996017.
[23] Li N, Cui C, Zhao Y, Zhang Q, Bai L. Structure and properties of GCr15 modified by multiphase ceramic nanoparticles/Fe-C composite inoculants. Mater Sci Eng: A 2018;738:63–74. https://doi.org/10.1016/j.msea.2018.09.074.